Interaction length-dependent saturable absorption of MoS_2-coated planarized waveguide and its effect on the performance of Q-switched pulse laser generation

Interaction length-dependent saturable absorption of MoS_2-coated planarized waveguide and its effect on the performance of Q-switched pulse laser generation

Jing Wen Chew, Kok Bin Ng, Soon Xin Gan, Lian Seng Tey, Wu Yi Chong, Yuen Kiat Yap, Harith Ahmad

***Abstract*— The performance of Q-switched erbium doped fiber laser using monolayer molybdenum disulfide (MoS_2)-coated planarized optical waveguides with different MoS_2 coating lengths is studied in this work. Monolayer MoS_2 thin film is integrated onto a planarized optical waveguide using dry transfer technique. As the MoS_2 thin film interacts with the evanescent field only, the MoS_2-coated planarized waveguide saturable absorber provides advantages in terms of high damage threshold and controllable interaction length between the MoS_2 thin film and the light propagating in the waveguide. With a MoS_2 coating length of 7.2 mm, the laser shows a widely tunable wavelength range of 38.6 nm. The wavelength tunability of the Q-switched fiber laser reduces to 5.9 nm when the interaction length between light propagating in the waveguide and the MoS_2 monolayer is reduced to 2.5 mm. This effect is attributed to the reduction in the number of vacancy states of MoS_2 in shorter length coatings. The results obtained contribute valuable information towards the development of all-planar waveguide pulsed laser source.**

***Index Terms*— Molybdenum disulfide, saturable absorber, evanescent field interaction, Q-switched laser.**

I. Introduction

Since the realization of the first optical waveguide in the early 1960s, research in waveguide-based photonics integrated circuit has been an active research field to date due to their wide range of useful applications, ranging from optical communications, sensors, lab-on-chip integration, etc. [1]-[3]. The factors contributing to these applications come mainly from the fact that optical waveguide technology provides flexibility in terms of fabrication technique, structural layout and compact footprint. Apart from that, many low-dimensional materials can be integrated onto an optical waveguide to produce multi-functional photonics integrated devices. For example, two-dimensional (2D) materials can be integrated into an optical waveguide to realize on-chip, compact pulsed laser sources [4]. Such 2D materials act as saturable absorber (SA) elements that modulate the optical mode in the waveguide to realize passively Q-switched or mode-locked pulsed waveguide lasers.

Owing to its atomic layer thickness and strong light-matter interaction, extensive studies have been carried out in utilizing 2D materials for pulsed laser generation [5]-[9]. They can be integrated with a waveguide in such a way that they are coated on or around the waveguide core to interact with the laser modes via evanescent field. Choudhary *et al.* realized a 2D graphene-based Q-switched waveguide laser at the 1.0 μm wavelength range through evanescent field interaction [10]. No optical damage was observed on the graphene SA despite a high pump power level of 4.1 W being applied to the waveguide laser. Meanwhile, Liu *et al.* demonstrated a graphene-based Q-switched waveguide laser using a Y-branch structure [11]. This further shows the flexibility of waveguide design warranted by evanescent field interaction to produce pulsed waveguide lasers. On the other hand, Ma *et al.* produces a Q-switched laser using 2D tungsten disulfide as SA on a ridge waveguide structure with a minimum pulse duration of 125 ns [12]. Evanescent field interaction allows the control of interaction length of the SA. Prior reports used millimeter and centimeter long SA coating to realize pulsed laser generation. However, there are limited works to systematically investigate the effect of interaction length of SA on the performance of pulsed laser generation [13]-[15].

In this paper, the effect of interaction length of SA coating on the performance of pulsed laser generation is investigated. A monolayer molybdenum disulfide (MoS_2) is used as the SA element. It is transferred onto a planarized optical waveguide using an all-dry viscoelastic stamping method. SAs with different MoS_2 coating lengths are produced. The SA performance of MoS_2-coated waveguides is studied using an erbium-doped fiber laser (EDFL) cavity. The generated Q-switched pulses show different characteristics with different SA interaction length. The information obtained from this study is essential in the design and development of compact, wavelength-tunable planar waveguide pulsed lasers.

This work is supported by the Ministry of Education of Malaysia, under Fundamental Research Grant Scheme (FRGS/1/2018/STG02/HWUM02/2). This study undertaken by Jing Wen Chew and Kok Bin Ng is supported by Malaysia's Ministry of Education via MyBrainSc scholarship.

J. W. Chew, K. B. Ng, S. X. Gan, L. S. Tey, W. Y. Chong and H. Ahmad are with Photonics Research Centre, University of Malaya, 50603 Kuala Lumpur, Malaysia; also with Department of Physics, Faculty of Science, University of Malaya, 50603 Kuala Lumpur, Malaysia (e-mail: wuyi@um.edu.my).

Y. K. Yap is with Heriot-Watt University Malaysia, Precinct 5, 62200 Putrajaya, Malaysia.

II. EXPERIMENTS

A. Characterization of the MoS_2 monolayer thin film

A CVD-grown monolayer MoS_2 on a polydimethylsiloxane (PDMS) substrate is purchased (6Carbon Technology). The PDMS acts as a viscoelastic stamp which enables easy and flexible transfer of the monolayer MoS_2 to the target planarized waveguide. The transferring process will be discussed in detail in the following section. The MoS_2-PDMS sample was characterized using Raman spectroscopy (*Renishaw* InVia micro-Raman spectrometer) using excitation wavelength and power of 532 nm and 0.25 mW, respectively. The Raman spectrum is shown in Fig. 1. Two characteristic peaks at 384.6 cm^{-1} and 405.2 cm^{-1} were observed, that correspond to the E_{2g} and A_{1g} modes of MoS_2, respectively. The spacing, Δ, between these modes is ~ 20.6 cm^{-1}, which corresponds to the Raman shift of monolayer MoS_2 [16],[17].

B. Characterization of the planarized waveguide

A planarized waveguide structure is used in this work. The planarized waveguide comprises of a germanium-doped silica core, surrounded by polymer side-cladding and thermal oxide under-cladding, with refractive indices of 1.486, 1.440 and 1.444, respectively. The physical length of the waveguide is 15 mm. The core has a dimension of 2.4×3 μm^2 that supports only fundamental mode light propagation at 1550 nm and allows effective evanescent field interaction between the coating and the top of the waveguide core [18]. The coupling of light into the waveguide is achieved using two single-mode optical fibers with mode field diameter of 3.8 μm (Nufern, UHNA4) as shown in Fig. 2. The alignment between optical fibers and waveguide are performed using a pair of five-axis linear translation stages. To reduce the Fresnel reflection loss from the fiber-waveguide interfaces, index matching fluid is applied on both fiber tips. The insertion loss of the waveguide is measured to be 6.25 dB. Care was taken to ensure that the index matching fluid is coated only on the fiber tips, but not on the waveguide surface.

C. Preparation of MoS_2-coated planarized waveguide

The MoS_2-coated waveguide is prepared by transferring a monolayer MoS_2 from its substrate (PDMS) to the target planarized waveguide using an all-dry viscoelastic stamping method [19]. The choice of PDMS as the substrate is essential as it can serve as the viscoelastic stamp. The stamping procedure was carried out using the set up shown in Fig. 3(a). Firstly, the MoS_2-PDMS sample was cut into three smaller pieces of 2.5 mm, 4.4 mm, 7.2 mm and 9.2 mm in length, using a sharp razor blade. These MoS_2-PDMS samples were then placed on a glass slide that is fixed on a three-axis linear translation stage, with the MoS_2 thin film facing down. With the help of a long working distance inspection scope, the sample was precisely aligned to the desired region on the target surface using the translation stage. After alignment was completed, the stamp was lowered down towards the target surface until it comes into contact with the surface firmly without any air bubble. The setup is left overnight before the stamp was peeled off. The MoS_2 thin film was then transferred successfully to the planarized waveguide. As shown in Fig. 3(b), the MoS_2 thin film coating on the planarized waveguide is visible with a slightly different contrast. The MoS_2 coating length is limited by the size of CVD-grown MoS_2, which is 10 mm × 10 mm. Also, transferring longer MoS_2 film may introduce discontinuity to the coating. Fig. 3(c) shows the optical micrograph of 9.2 mm MoS_2 film transferred onto the waveguide, where delamination of MoS_2 coating can be observed. This may affect the saturable absorption performance of the MoS_2-coated waveguide.

Loss measurements were carried out on the MoS_2 coated planarized waveguides, and we find that the MoS_2 thin film coatings introduce less than 0.5 dB of insertion loss and polarization dependent loss to the planarized waveguides. These MoS_2-coated waveguides act as the SAs and will be used for the pulsed laser generation. In the discussion later, the MoS_2-coated waveguides with interaction length of 2.5 mm, 4.4 mm, 7.2 mm and 9.2 mm were labelled as SA1, SA2, SA3 and SA4, respectively.

D. Characterization of the nonlinear transmission of the SAs

The nonlinear transmission of the SAs are measured using a twin detector measurement technique, as shown in Fig. 4(a). A homemade 1531 nm ns-pulse laser is used as the pump source. The repetition rate and pulse width are 10 kHz and 30 ns, respectively. The power of the laser is controlled by a variable optical attenuator (VOA). The source is coupled into a 50/50 optical coupler (OC), with one arm connected with the SAs. The average power of both arms is measured using two OPMs.

E. Characterization of the Q-switched laser

The Q-switched fiber laser cavity is shown in Fig. 4(b). A 980 nm diode laser is used as the pump source and its power is delivered to the erbium-doped fiber (EDF) through a 980/1550 wavelength division multiplexer (WDM). An EDF (LIEKKI Er110-4/125) with a length of 0.62 m is used as the gain medium. An optical isolator (ISO) is spliced after the EDF to ensure uni-directional laser propagation in the cavity. A polarization controller (PC) is used to control the polarization state of the laser. An etalon-based tunable bandpass filter (TBF) is connected after the PC to select the oscillation wavelength. The wavelength of the TBF can be tuned from 1510 nm to 1590 nm. The SA is inserted into the laser cavity after the TBF. As aforementioned, laser light is coupled into the SA using two single-mode optical fiber tips on two five-axis linear translation stages. The laser output is routed out via an 80/20 OC, where 80% of light power is feedback into the cavity while 20% of it is coupled out for characterization. The generated Q-switched pulse train is recorded by a photodiode (Thorlabs PDA50B-EC) connected to an oscilloscope (OSC). The average output power and optical spectrum of the pulsed laser are measured using an optical power meter (OPM, Thorlabs S144C) and optical spectrum analyzer (OSA, YOKOGAWA AQ6370),

respectively.

III. RESULTS AND DISCUSSION

The nonlinear transmission curves of the SAs are depicted in Fig. 5. In Fig. 5, typical saturable absorption profiles are obtained for all the SAs. With increasing peak intensity, the absorption of the SA decreases and saturates after ~ 0.3 MW/cm^2. The intensity dependent transmission, $T(I)$, is fitted using the equation $T(I) = 1 - {\alpha_s}/{1 + (I/I_{sat})} + \alpha_{ns}$, where α_s is the modulation depth, α_{ns} is the non-saturable loss, I and I_{sat} are the intensity of the pump source and saturation intensity, respectively. The α_s of SA3 is ~ 0.9%, which is more than 3 times larger compared to SA1, SA2, and SA4. This indicates that SA3 has a higher saturable absorption, which can lead to a better pulse shaping ability. Besides, the I_{sat} of SA3 is 64.9 kW/cm^2, which is lower than the other SAs as well.

The lasing wavelength is initially fixed at 1531 nm using the TBF. When the pump power is low, the laser cavity operates in continuous wave regime. As the pump power is increased, stable Q-switched laser pulses can be observed. Similar behaviour was observed for all four SAs. The threshold pump power for Q-switched operation of SA1 is 88.7 mW, whereas SA2, SA3 and SA4 are 77.4 mW. It should be noted that without MoS_2 coating on the waveguide, no stable pulse is observed for all laser pump power levels. We do not observe mode-locking generation in the current setup, which may be due to the large insertion loss of the SAs. However, this is not an issue in an integrated all-planar waveguide laser platform, where laser coupling between the waveguide and fibers is not necessary.

Fig. 6(a) illustrates the Q-switched pulse trains produced using the four SAs at pump power of 100 mW. The pulse train produced by the SAs have different repetition rate, f. The pulses generated by SA1 has a pulse duration, τ_p, of 10.9 µs. For SA2, SA3 and SA4, their τ_p are 7.5 µs, 7.3 µs and 7.7 µs, respectively. Moreover, the f decreases slightly from SA4 to SA1. These observations indicate that longer interaction length of MoS_2 improves the performance of Q-switched lasers in terms of higher f and shorter τ_p. Their corresponding radio-frequency (RF) spectra are shown in Fig. 6(b). The RF spectrum of SAs shows an increasing trend of signal-to-noise ratio (SNR) from SA1 to SA4. For instance, SA4 has a SNR of 45 dB, whereas SA1 has a SNR of 38 dB.-These observations again indicate that the longer interaction length could provide a better pulse stability. Despite of that, the RF spectra produced by all SAs are regular and do not show spectral modulation, inferring that the Q-switched lasers are stable for practical applications.

The evolution of f and τ_p, of the Q-switched lasers as a function of pump power at a fixed wavelength of 1531 nm are shown in Fig. 7. Based on Fig. 7(a), it is obvious that SA3 generates pulsed laser over a larger pump power range compared to SA1, SA2 and SA4. For example, SA3 produces stable Q-switched laser for pump powers ranging from 77.4 mW to 190.9 mW. Above this pump power, the pulse train becomes unstable and disappear eventually. For SA1, SA2 and SA4, stable Q-switched operation occur at a smaller pump power range. In Fig. 7(a), the f of the Q-switched pulses increases monotonically with the pump power for SA3, from 6.6 kHz at 77.4 mW to 40.2 kHz at 190.9 mW. On the other hand, the variation of f of the pulsed laser produced by SA1, SA2 and SA4 show similar trend, in which they increase linearly with the pump power. The maximum achievable f of SA1, SA2 and SA4 are 24.8 kHz, 23.9 kHz and 25.8kHz, respectively. Meanwhile, the τ_p of SAs show a typical Q-switching characteristic as well, in which it decreases with increasing pump power. The shortest achievable τ_p of SA3 is 2.9 µs when the pump power is set to 168.2 mW. From Fig. 7(b), it is found that the overall τ_p of SA3 is shorter than that of other SAs. For instance, the shortest τ_p of SA3 (2.9 µs) is 2.9 times shorter than that of SA1 (8.3 µs).

The average output power, P_{out} of the pulsed laser increases linearly with pump power as depicted in Fig. 8(a). Generally, the P_{out} of SA3 is slightly larger than that of SA1, SA2 and SA4. The maximum attainable output power, $P_{out,max}$, of SA3 is 0.22 mW at 190.9 mW pump power. As a comparison, the $P_{out,max}$ produced by SA1 is 45 µW at 128.5 mW pump power. From Fig. 8(b), it can be seen that the pulse energy, E_p of SA3 increases as the pump power increases until 174 mW. After 174 mW, the E_p becomes saturated. The maximum E_p generated is 6 nJ at this pump power. The E_p of SA3 is much larger than the maximum attainable pulse energy of SA1, SA2 and SA4, which gives the value of 1.8 nJ, 2.5 nJ and 3.0 nJ, respectively, at lower pump power. We note that the generated P_{out} and E_p of the Q-switched laser is low [20, 21]. This may be due to the large insertion loss from the fiber-waveguide-fiber couplings. Nonetheless, this will not be an issue when the MoS_2 is integrated onto an all-planar waveguide laser. Furthermore, based on both Fig. 7 and Fig. 8, it is interesting to find that the performance of Q-switching does not scale monotonically with the MoS_2 coating length. For instance, the P_{out} and E_p of SA4 is lower than that of SA3, though the coating length is the longest. The possible reason might be due to the inferior coating quality, which limit the performance of the Q-switching.

To investigate the wavelength tunability of SAs, the pump power was fixed at 88.7 mW (100 mW for SA1) – which is about 10 mW above threshold pump power when stable Q-switching were initiated - and the laser wavelength were tuned using the TBF. Fig. 9(a) demonstrates the optical spectra of each SA measured by OSA when Q-switched pulsed laser is produced. From Fig. 9(a), the lasing wavelength of the Q-switched laser by SA3 is widely tunable, ranging from 1527 nm to 1565.6 nm, limited only by the gain bandwidth of the EDF. Meanwhile, the lasing wavelength of SA1, SA2 and SA4 range from 1528 – 1533.9 nm, 1526 – 1535.6 nm and 1526.4 – 1536 nm, respectively. Fig. 9(b) shows the Q-switching wavelength range of the SAs. The operating wavelength range of SA3 and SA1 are 38.6 nm and 5.9 nm, respectively. This shows that the operating wavelength range of SA3 is 6.5 times broader than that produced using SA1. Again, the Q-switching wavelength range of SA4 is not the broadest. This will be discussed in the paragraph below.

The superior performance of SA3 can be attributed to the

difference in the number of defects in the MoS_2 thin film. The longer MoS_2 coating length increases the interaction between the light in the waveguide with the number of defects in the MoS_2 thin film. The presence of defects in monolayer MoS_2 plays an important contribution to sub-bandgap saturable absorption in the 1550 nm wavelength range [6]. It should be noted that although MoS_2 thin films grown using CVD method appears uniform and homogeneous upon optical inspection, defects can still be present within the thin film [22]. CVD process may produce sulphur (S) vacancies defect in the MoS_2 thin film [23]. These vacancies change the bandgap, and hence the optical properties of MoS_2. Kunstmann *et al.* shows that the S (V_s) and 2S (V_{2S}) vacancies introduce absorption peaks at energies smaller than 1.9 eV (the bandgap energy of perfect monolayer MoS_2 crystal) [24]. The increase of vacancy density will increase the absorption of sub-1.9 eV photons as well. For example, with 11.1% of V_{2S}, large absorption peak at ~ 1.1 eV (corresponds to ~ 1.13 μm wavelength) is observed, and the absorption reduces rapidly to zero at ~ 0.7 eV (~ 1.77 μm wavelength). On the other hand, 25% V_{2S} causes strong absorption peak at 0.88 eV (~ 1.41 μm wavelength) that reduces in strength towards ~ 0.6 eV (~ 2.07 μm wavelength) [24]. We anticipate that the concentration of sulphur vacancies affects the wavelength range for Q-switching as well, since saturable absorption involves the transition of electrons from the sub-bandgaps of MoS_2. Compared to SA1, SA3 has longer interaction length between the planarized waveguide and MoS_2 thin film, which increases the number of vacancies along the MoS_2-coated waveguide and therefore extending the sub-bandgap absorption to the longer wavelength. This may be the reason that the Q-switched lasing wavelength of the EDFL using SA3 extends to ~ 1565 nm, while SA1 can only produce Q-switching over a relatively narrower wavelength range. The narrower lasing wavelength of SA4 may possibly come from the inferior coating quality. This increases the exposed (or terminated) edge sites of MoS_2 coating due to the delamination of MoS_2 coating on the waveguide, as shown in Fig. 3(c). In other words, this increases the ratio of exposed edge-to-vacancy compared to others. The exposed edges of MoS_2 will be passivated by other element to form a stable structure [25]. Javaid *et al.* shows that the passivated MoS_2 edge has a wider bandgap [25]. This may cause a reduced saturable absorption of SA4 at longer wavelength.

To verify this point, the optical transmission spectra of the SAs across the wavelength range from 1500 nm to 1600 nm were measured and shown in Fig. 10. It can be seen that transmission spectra for all SAs increase towards the longer wavelengths. In addition, the absorption of SA3 is higher than that of other SAs. The lower optical absorption for SA1 can be attributed to the lower number of V_{2S} vacancies – as discussed earlier – and results in the inability of SA1 to produce Q-switched laser pulses towards the longer wavelength range. On the other hand, SA4 exhibits lower absorption at longer wavelength, which limits the Q-switching lasing wavelength range as shown in Fig. 9(b). Therefore, long interaction length of the MoS_2 coating with minimum exposed edge site plays an important role in producing Q-switched pulses with wider operating wavelength tunability.

IV. Conclusion

MoS_2-coated planarized waveguide SAs have been fabricated by transferring the monolayer MoS_2 thin films, with different lengths, onto the planarized waveguide using an all-dry stamping method. The interaction length dependent Q-switching performance of the SAs were studied using an EDFL. The Q-switching performance improves with longer coating length up to 7.2 mm, which can be attributed to the increase in the overall number of vacancy states of the MoS_2 thin film coating. For longer coating length, Q-switching performance deteriorates due to delamination of the MoS_2 coating caused by the current film transfer setup. The information attained will pave a route for the development of all-planar waveguide laser applications.

References

[1] E. Snitzer, "Optical maser action of ND+3 in a barium crown glass," Physical Review Letters, vol. 7, no. 12, p. 444, Dec. 1961.

[2] G. Lifante, "Introduction to integrated photonics," in *Integrated photonics: fundamentals*. John Wiley & Sons, 2003, pp. 1–21.

[3] C. Grivas, "Optically pumped planar waveguide lasers: Part II: Gain media, laser systems, and applications," *Progress in Quantum Electronics*, vol. 45, pp. 3–160, Jan. 2016.

[4] Z. Li, C. Pang, R. Li, and F. Chen, "Low-dimensional materials as saturable absorbers for pulsed waveguide lasers," *Journal of Physics: Photonics*, vol. 2, no. 3, p. 031001, May. 2020.

[5] S. Yu, X. Wu, Y. Wang, X. Guo, and L. Tong, "2D materials for optical modulation: challenges and opportunities," *Advanced Materials*, vol. 29, no. 14, p. 1606128, Feb. 2017.

[6] R. Woodward, E. Kelleher, R. Howe, G. Hu, F. Torrisi, T. Hasan, S. Popov, and J. Taylor, "Tunable Q-switched fiber laser based on saturable edge-state absorption in few-layer molybdenum disulfide (MoS2)," *Optics express*, vol. 22, no. 25, pp. 31113–31122, Dec. 2014.

[7] D. Mao, Y. Wang, C. Ma, L. Han, B. Jiang, X. Gan, S. Hua, W. Zhang, T. Mei, and J. Zhao, "WS2 mode-locked ultrafast fiber laser," *Scientific reports*, vol. 5, p. 7965, Jan. 2015.

[8] H. Zhang, S. Lu, J. Zheng, J. Du, S. Wen, D. Tang, and K. Loh, "Molybdenum disulfide (MoS2) as a broadband saturable absorber for ultra-fast photonics," *Optics express*, vol. 22, no. 6, pp. 7249-7260, Mar. 2014.

[9] Z. Sun, T. Hasan, F. Torrisi, D. Popa, G. Privitera, F. Wang, F. Bonaccorso, D. M. Basko, and A. C. Ferrari, "Graphene mode-locked ultrafast laser," *ACS nano*, vol. 4, no. 2, pp. 803–810, Jan. 2010.

[10] A. Choudhary, S. J. Beecher, S. Dhingra, B. D'Urso, T. L. Parsonage, J. A. Grant-Jacob, P. Hua, J. I. Mackenzie, R. W. Eason, and D. P. Shepherd, "456-mW graphene Q-switched Yb:yttria waveguide laser by evanescent-field interaction," Optics Letters, vol. 40, no. 9, pp. 1912–1915, May. 2015.

[11] H. Liu, C. Cheng, C. Romero, J. R. V. de Aldana, and F. Chen, "Graphene-based Y-branch laser in femtosecond laser written Nd:YAG waveguides," Optics Express, vol. 23, no. 8, pp. 9730–9735, Apr. 2015.

[12] L. Ma, Y. Tan, S. Wang, S. Akhmadaliev, S. Zhou, H. Yu, H. Zhang, and F. Chen, "Continuous-wave and Q-switched Yb:YSGG waveguide laser," *Journal of Lightwave Technology*, vol. 35, no. 13, pp. 2642–2645, Dec. 2017.

[13] D. Fan, C. Mou, X. Bai, S. Wang, N. Chen, and X. Zeng, "Passively Q-switched erbium-doped fiber laser using evanescent field interaction with

gold-nanosphere based saturable absorber," *Optics express*, vol. 22, no. 15, pp. 18537–18542, Jul. 2014.

[14] R. Khazaeinezhad, S. H. Kassani, H. Jeong, K. J. Park, B. Y. Kim, D. Yeom, K. Oh, "Ultrafast pulsed all-fiber laser based on tapered fiber enclosed by few-layer WS2 nanosheets," *IEEE Photonics Technology Letters*, vol. 27, no. 15, pp. 1581–1584, Aug. 2015.

[15] Y. Jia and F. Chen, "Compact solid-state waveguide lasers operating in the pulsed regime: a review," *Chinese Optics Letters*, vol. 17, no. 1, p. 012302, Jan. 2019.

[16] H. Li, Q. Zhang, C. C. R. Yap, B. K. Tay, T. H. T. Edwin, A. Olivier, and D. Baillargeat, "From bulk to monolayer MoS2: evolution of Raman scattering," *Advanced Functional Materials*, vol. 22, no. 7, pp. 1385–1390, Jan. 2012.

[17] S. Li, H. Miyazaki, H. Song, H. Kuramochi, S. Nakaharai, and K. Tsukagoshi, "Quantitative Raman spectrum and reliable thickness identification for atomic layers on insulating substrates," *ACS nano*, vol. 6, no. 8, pp. 7381–7388, Jul. 2012.

[18] S. X. Gan, C. K. Lai, W. S. Chong, W. Y. Chong, S. Madden, and H. Ahmad, "Large polarization response of planarized optical waveguide functionalized with 2D material overlays," *Journal of Modern Optics*, vol. 67, no. 8, pp. 730-736, May 2020.

[19] A. Castellanos-Gomez, M. Buscema, R. Molenaar, V. Singh, L. Janssen, H. S. Van derZant, and G. A. Steele, "Deterministic transfer of two-dimensional materials by all-dry viscoelastic stamping," *2D Materials*, vol. 1, no. 011002, Apr. 2014.

[20] H. Li, H. Xia, C. Lan, C. Li, X. Zhang, J. Li, and Y. Liu, "Passively Q-switched erbium-doped fiber laser based on few-layer MoS2 saturable absorber," *IEEE Photonics Technology Letters*, vol. 27, no. 1, pp. 69–72, Oct. 2014.

[21] Y. Huang, Z. Luo, Y. Li, M. Zhong, B. Xu, K. Che, H. Xu, Z. Cai, J. Peng, and J. Weng, "Widely-tunable, passively Q-switched erbium-doped fiber laser with few-layer MoS2 saturable absorber," *Optics Express*, vol. 22, no. 21, pp. 25258–25266, Oct. 2014.

[22] X. Yin, Z. Ye, D. A. Chenet, Y. Ye, K. O'Brien, J. C. Hone, and X. Zhang, "Edge nonlinear optics on a MoS2 atomic monolayer," *Science*, Vol. 344, no. 6183, pp. 488–490, May. 2014.

[23] M. Pandey, F. A. Rasmussen, K. Kuhar, T. Olsen, K. W. Jacobsen, and K. S. Thygesen, "Defect-tolerant monolayer transition metal dichalcogenides," *Nano letters*, vol. 16, no. 4, pp. 2234–2239, Mar. 2016.

[24] J. Kunstmann, T. B. Wendumu, and G. Seifert, "Localized defect states in MoS2 monolayers: Electronic and optical properties," *physica status solidi*, vol. 254, no. 4, p. 1600645, Oct. 2017.

[25] M. Javaid, D. W. Drumm, S. P. Russo, and A. D. Greentree, "A study of size-dependent properties of MoS2 monolayer nanoflakes using density-functional theory," *Scientific reports*, vol. 7, no. 1, pp. 1-11, August 2017.

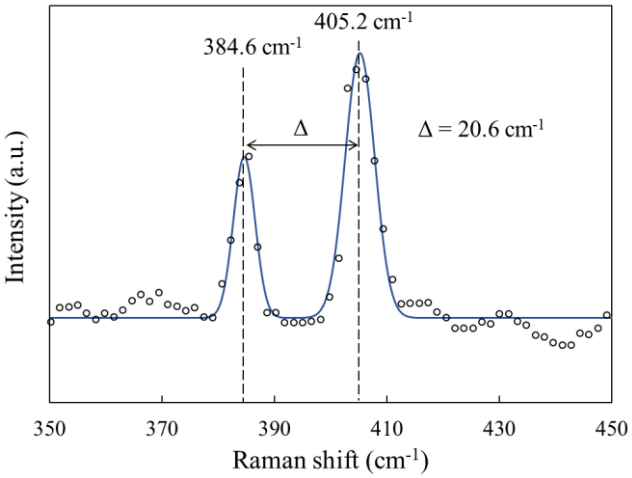

Fig. 1. Raman spectrum of MoS_2 sample. The solid line is a Gaussian fitting line as a guide to the raw data. The spacing between the two characteristic E_{2g} and A_{1g} modes is ~ 20.6 cm^{-1}, indicating that the MoS_2 sample consists of a monolayer.

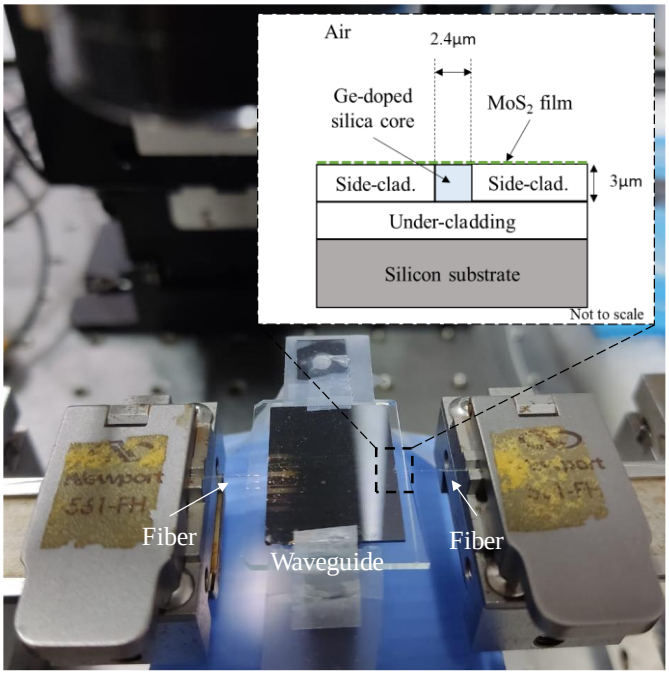

Fig. 2. Setup of optical fiber-waveguide coupling. Inset: cross-sectional schematic diagram of the planarized waveguide.

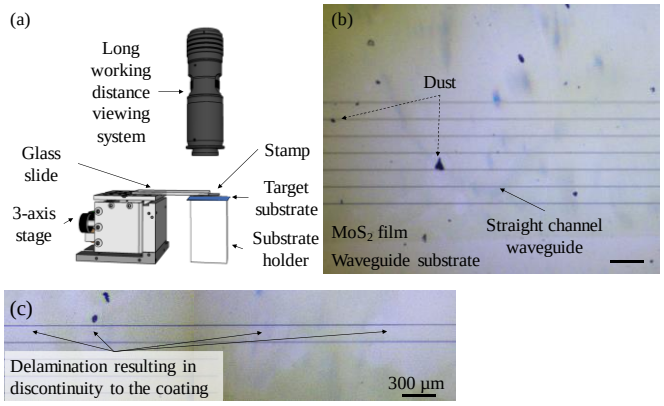

Fig. 3. (a) Schematic setup for the all-dry viscoelastic stamping technique. (b) Optical micrograph of the transferred MoS_2 on the planarized waveguide. The MoS_2 film covers a large portion of the straight waveguides. The scale bar is 200 μm. (c) Optical micrograph of 9.2mm transferred MoS_2 with delamination.

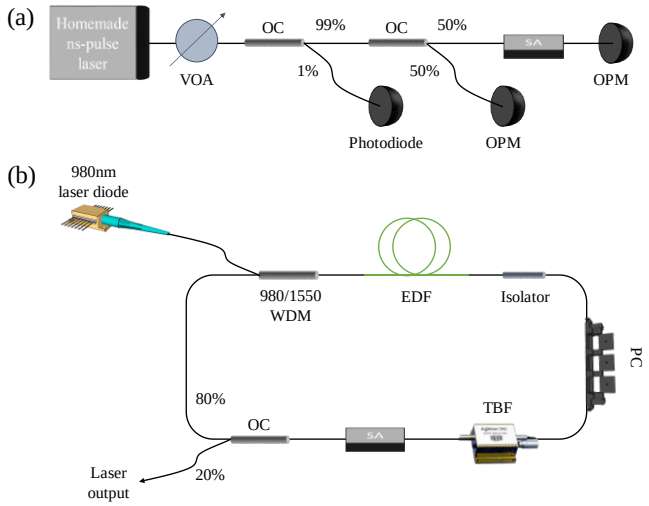

Fig. 4. The schematic arrangement of: (a) the twin detector measurement technique; and (b) the fiber laser cavity.

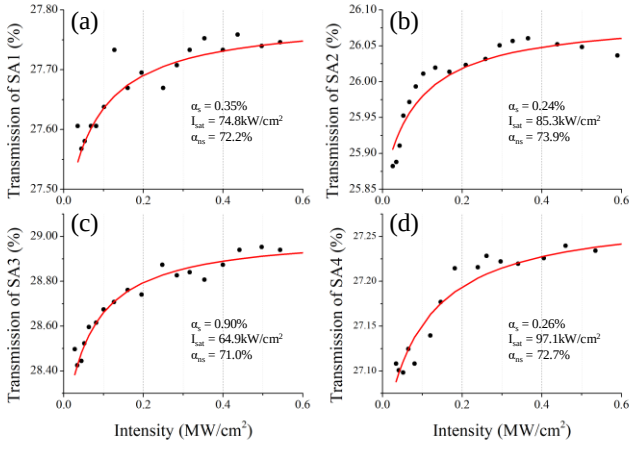

Fig. 5. The graph of nonlinear transmission of (a) SA1; (b) SA2; (c) SA3; and (d) SA4. The black, solid dots represent the raw data obtained from the experiment, whereas the red, solid curves represent the fitting curve.

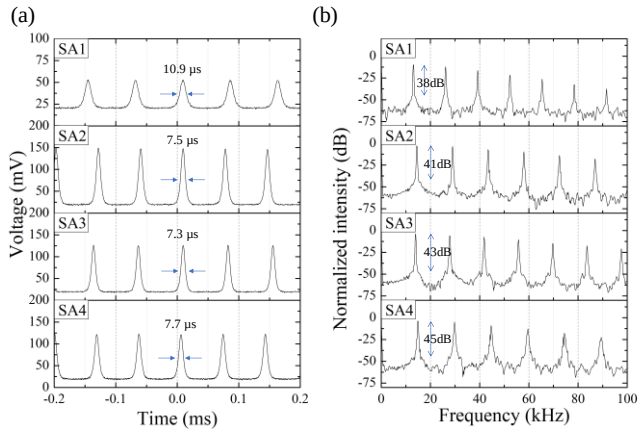

Fig. 6. (a) Q-switched pulse train of SAs; (b) RF spectra of the SAs at a fixed wavelength and pump power of 1531 nm and 100 mW, respectively.

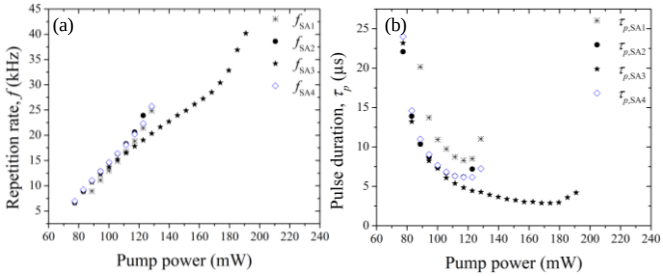

Fig. 7. Evolution of (a) f and (b) τ_p of SAs against pump power.

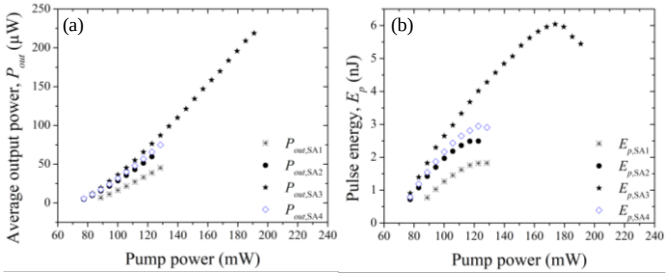

Fig. 8. Development of (a) P_{out} and (b) E_p of SAs against pump power.

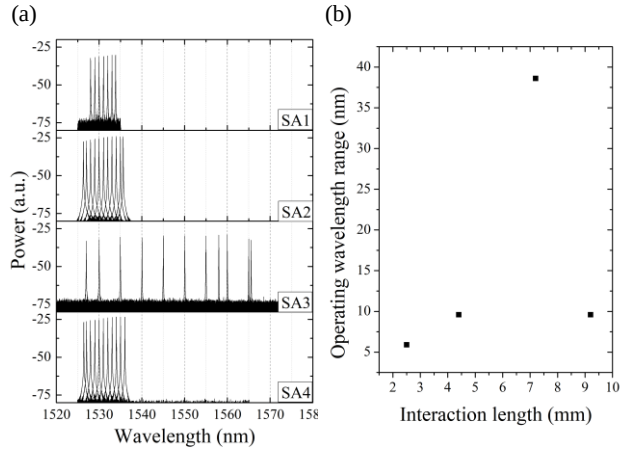

Fig. 9. (a) The spectra of Q-switched EDFL using different SAs, indicating the respective wavelength tuning range of each SAs ; (b) relationship between operating wavelength range and coating length of MoS_2 on the waveguide in producing Q-switched laser.

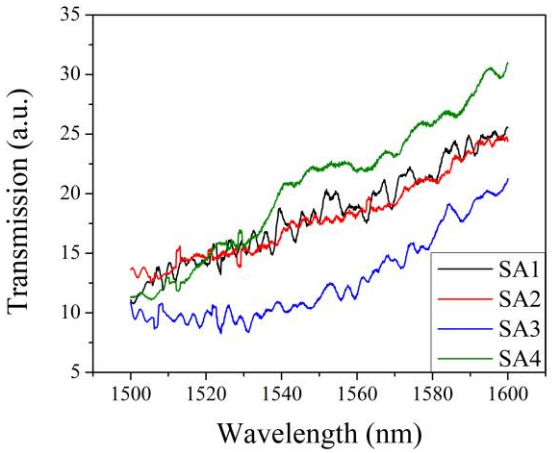

Fig. 10. Optical transmission spectra of SAs across 1500 – 1600 nm.

Jing Wen Chew received the B.S. degrees in physics from the Department of Physics, Faculty of Science, University of Malaya, Federal Territory of Kuala Lumpur, Malaysia, in 2018. He is currently pursuing his Ph.D. in the same institution.

He is the author of two articles. His research interests include optical nonlinearity studies of two-dimensional transition metal dichalcogenides using high peak power pulsed lasers, its preparation, basic characterization and integration method on optical waveguides.

Kok Bin Ng received the B.S. degrees in physics from the Department of Physics, Faculty of Science, University of Malaya, Federal Territory of Kuala Lumpur, Malaysia, in 2018. He is currently pursuing his Ph.D. in the same institution.

His research interests include ultrafast laser processing of materials, for instance, ultrafast pulsed laser ablation and the development of a complex optical waveguide fabrication system using an ultrafast direct laser writing technique on various polymer materials.

Soon Xin Gan received the B.S. degrees in physics from University of Malaya (UM), Federal Territory of Kuala Lumpur, Malaysia, in 2017, and the M.S. degree in Experimental Physics (Photonics) from UM in 2020. He is currently pursuing his Ph.D. in Experimental Physics in the same institution.

During his M.S. degree, his research interests include the development of graphene oxide functionalized integrated optics such as waveguide-based polarizer and all-optical switch. For his current Ph.D. studies, his research focuses on the development of nonvolatile all-optical switch and photonic memory based on the integration of graphene oxide and phase change material.

Lian Seng Tey received the B.S. degrees in physics from the Department of Physics, Faculty of Science, University of Malaya, Federal Territory of Kuala Lumpur, Malaysia, in 2021. He is currently pursuing his PhD in the same institution.

From 2021 to 2022, he was a Research Assistant with the Department of Physics, University of Malaya. His research interests include the single photon generation and detection, dual quantum-classical transport dynamics and quantum information processing.

Wu Yi Chong received the B.S. degrees in physics from University of Malaya in 2003. He obtained his M.S. and Ph.D. degrees from the same institution in 2001 and 2011, respectively.

He is currently a senior lecturer at the University of Malaya. He has been involved in the research of fiber amplifiers and planar lightwave circuit fabrication. His current research interests include direct laser writing, optical waveguide sensing as well as fabrication of integrated optics.

Yuen Kiat Yap received the Ph.D. degrees in laser and photonics from University of Malaya, Federal Territory of Kuala Lumpur, Malaysia.

He researches in fiber photonics, with themes of optical materials, ultrafast laser and waveguide photonics. His current interest is in high peak power short pulse laser for table-top pump-probe dynamics.

Harith Ahmad graduated from University of Malaya (UM) in 1979. He received the M.S. and Ph.D degrees from the University of Wales in 1980 and 1983, respectively.

He became a member of the academic staff of UM in 1983, where he is now a distinguished professor and the director of the Photonics Research Centre of the University of Malaya. His research interests include ultrafast fiber laser generation, two-dimensional optical materials, and nonlinear optics.